Reduced Holey Graphene Oxide Membranes for Desalination with Improved Water Permeance

Xiaoyi Chen,[1] Zhihao Feng,[1] Janavi Gohil,[1] Christopher M. Stafford,[2] Ning Dai,[3]

Liang Huang,[1*] and Haiqing Lin[1*]

[1] Department of Chemical and Biological Engineering, University at Buffalo, The State University of New York, Buffalo, NY 14260, USA

[2] Materials Science & Engineering Division, National Institute of Standards and Technology, MS 8542, 100 Bureau Drive, Gaithersburg, MD 20899, USA

[3] Department of Civil, Structural and Environmental Engineering, University at Buffalo, The State University of New York, Buffalo, NY 14260, USA

* Corresponding author. Tel: +1-716-645-1856, Email: haiqingl@buffalo.edu (H. Lin); lhuang28@buffalo.edu (L. Huang)

ABSTRACT

Reduced-graphene oxide (r-GO) membranes with narrow channels exhibit salt rejections comparable to conventional nanofiltration (NF) membranes. However, their water permeances are much lower because of the high tortuosity for water permeation. Herein we report a facile solution-processable approach to create in-plane nanopores on GO nanosheets before reduction, dramatically decreasing the tortuosity and increasing water permeance while retaining the salt rejection. Specifically, holey GO (HGO) nanosheets were prepared via chemical etching using hydrogen peroxide, followed by the deposition on a porous support by vacuum filtration and then reduction via exposure to hydriodic acid solutions to generate the reduced HGO (r-HGO) membrane. The generation of nanopores increases the water permeance from 0.4 L m^{-2}·h^{-1}·bar^{-1} (LMH/bar) to 6.6 LMH/bar with Na_2SO_4 rejection greater than 98.5 %, and the membranes were robust under strong cross-flow shearing force for 36 h. Both water permeance and Na_2SO_4 rejection of these r-HGO membranes for the first time simultaneously reach the level of the commercial polyamide-based NF membranes. Given their good antibacterial properties and resistance to aggressive chemical washing, the r-HGO membranes show the promise as next-generation NF membranes for desalination.

KEYWORDS: Holey graphene oxide; membranes; etching by H_2O_2; reduction by HI; desalination

1. INTRODUCTION

Two-dimensional (2D) sheets with atomic thickness are ideal membranes for water purification because of their potential in forming sub-10 nm layers with high water permeance.[1-3] For example, single-layer graphene with nanopores deposited on ultrafiltration (UF) membranes exhibited both high water permeance and salt rejection.[4-7] However, it remains challenging to synthesize large-area defect-free sheets and generate pores with high density and uniform pore sizes.[8] One approach to overcome these barriers is to prepare oxidized graphene (i.e., graphene oxide or GO), which can be stacked providing sub-nanometer interlayer channels (< 0.7 nm) for molecular separations.[9-11] Similar to graphene, in-plane nanopores can be generated on the GO sheets (holey GO or HGO) to reduce the tortuosity and thus increase water permeance.[12-14] However, the interlayer channels in GO or HGO are often larger than hydrated ions,[15-17] and thus, they are mainly investigated for dye removal (larger than 1 nm) or separation of organic solvents, instead of water desalination.[9, 18, 19] Additionally, GO is susceptible to re-dispersion in water due to its hydrophilicity and the shearing force from the feed flow, making it challenging for long-term underwater operation.

To improve stability and salt rejection, GO nanosheets can be reduced to partially remove hydrophilic oxygen-containing groups (reduced GO or r-GO), which increases hydrophobicity and decreases interlayer spacing.[20, 21] For instance, when GO was reduced by hydriodic acid (HI) vapor, increasing the exposure time from 0 to 3 min reduced the layer interspacing from 1.15 nm to 0.37 nm and thus water permeance from 11 L m^{-2} h^{-1} bar^{-1} (LMH/bar) to ≈2 LMH/bar, while the NaCl rejection increased from 28.6 % to 56.9 %.[20] There exhibits a trade-off between

stability and water permeability for these r-GO membranes, i.e., a higher degree of reduction (or greater stability and higher salt rejection) leads to a lower water permeance.[12]

An effective way to break this tradeoff is to create in-plane nanopores on r-GO sheets to decrease tortuosity and thus increase water permeance without decreasing salt rejection. For example, the membranes fabricated with HGO prepared using 70 % HNO_3 and then H_2 reduction (with Pd catalyst) exhibited water permeance of 5.3 LMH/bar and Na_2SO_4 rejection of less than 69 %.[11] Recently, HGO was prepared by chemical etching using hydrogen peroxide (H_2O_2), a mild process with flexibility in manipulating the pore size and density[22, 23] as compared to conventional methods such as electron beam/laser irradiation,[24, 25] catalytic oxidation,[14, 26, 27] thermal annealing,[28] and strong base and acid treatment.[11, 29, 30] The HGO was dried for 12 h and then thermally reduced at 150 ºC in the air for 1.5 h, and the obtained membranes exhibited water permeances of 40 LMH/bar and Na_2SO_4 rejection of ≈90 %.[23] However, the Na_2SO_4 rejection is still lower than conventional NF membranes (>98%), and the drying and annealing in the air may not be well-integrated into membrane manufacturing processes due to potential pore collapse of the support UF membrane.

Herein we demonstrate a solution-processable approach to prepare reduced HGO (r-HGO) membranes with desirable pore size and density. HGO was prepared using H_2O_2 etching and facilely dispersed in aqueous solutions, which was then vacuum-filtered on UF membranes and subsequently reduced using HI solutions at ≈22 ºC. The whole process uses aqueous solutions and can be scalable. Depending on the etching and reduction conditions, the obtained membranes exhibit water permeances ranging from 0.63 LMH/bar to 30 LMH/bar and Na_2SO_4

rejection ranging from 99.1 % to 82.8 %. The membranes show stable performance under crossflow with a strong shearing force for 36 h. We also prepared dual-layer r-HGO membranes with various degrees of etching and reduction and superior desalination performance. This work presents the first example of graphene-based membranes achieving both water permeance and Na_2SO_4 rejection similar to the commercial polyamide-based NF membranes (which has been optimized for more than 50 years).

2. RESULTS AND DISCUSSION

2.1. Synthesis and characterization of membranes

Figure 1a displays the process used for synthesizing r-HGO membrane, including the chemical etching of GO, preparation of HGO membranes by vacuum filtration, and reduction by HI solutions. The r-HGO membranes exhibit significantly less tortuosity for water permeation than the conventional r-GO membranes because of the holes in the HGO sheets. The subsequent reduction of the HGO by HI decreases the channel size and increases stability. The membranes are denoted as r-HGO-*x*-*y*, where *x* (h) is the H_2O_2 etching time for HGO formation, and *y* (mass%) is the HI concentration in the reduction solutions. The thickness of the HGO layer in this study is ≈20 nm unless otherwise stated.

Figure 1b compares the FTIR spectra of the synthesized GO, HGO, and r-HGO. Both GO and HGO exhibit characteristic peaks of functional groups, such as 3300 cm^{-1} (O-H stretching), 1720 cm^{-1} (stretching of C=O bond in –COOH), 1388 cm^{-1} (C-H bending), 1222 cm^{-1}

(stretching of C-O), and 1053 cm^{-1} (stretching of C-OH).[31, 32] By contrast, most of these peaks disappear in the r-HGO, confirming the removal of the oxygen-containing groups.

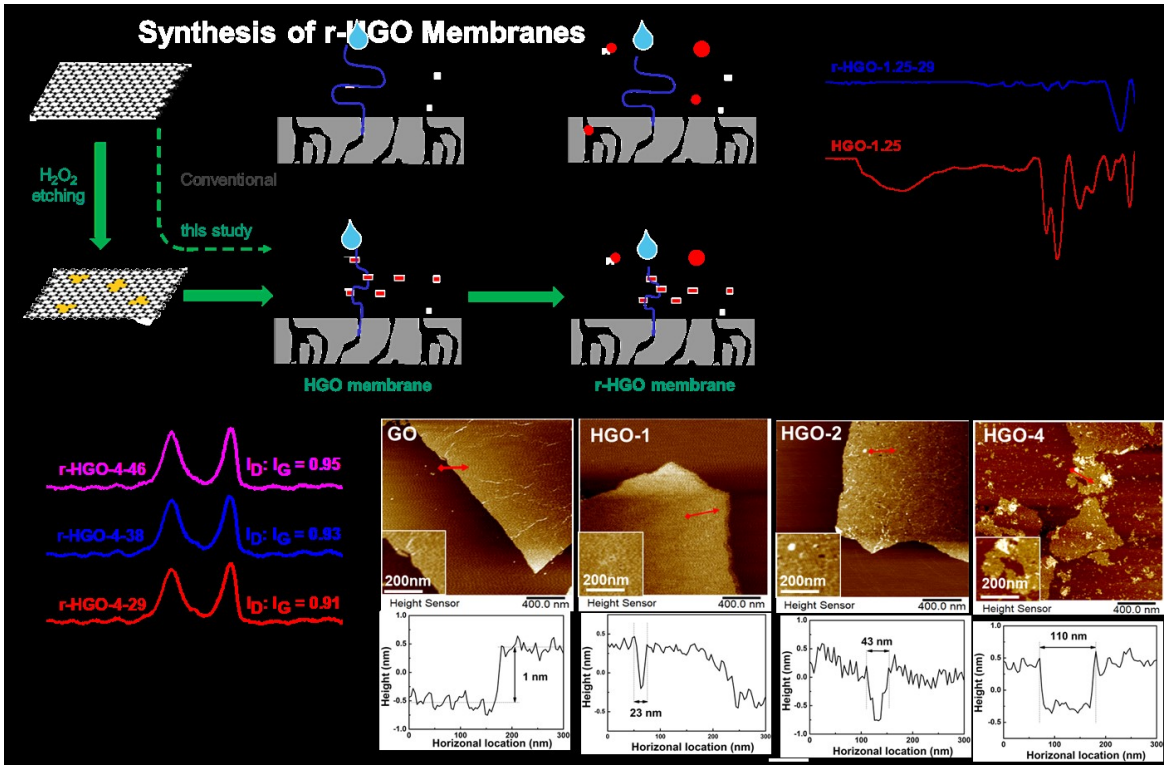

Figure 1. Synthesis and characterization of r-HGO. (a) Schematic of the synthesis of r-HGO membranes. (b) Fourier-transform infrared (FTIR) spectra of freestanding films of GO, HGO-1.25, and r-HGO-1.25-29. (c) Raman spectra of freestanding films of GO and r-HGO-4 samples. (d) Atomic force microscopy (AFM) images for HGO at various etching times. The red arrow shows the location where the magnified details and the corresponding height profiles are presented.

Figure 1c compares Raman spectra of the GO and r-HGO-4 samples, which display two characteristic peaks of 1350 cm^{-1} (D band) and 1600 cm^{-1} (G band) corresponding with the defects in the graphitic domains and the in-plane sp^2 domains, respectively.[19] For r-HGO samples, the I_D/I_G value increases with increasing HI concentration during reduction (or degree of reduction). The graphitic crystallite size (L_a) in the nanosheets can be estimated using the Tuinstra-Koenig equation ($L_a = 4.4 I_G/I_D$).[33, 34] The L_a value is 5.8 nm for GO and decreases

to decreases to 4.8 nm, 4.7 nm, and 4.6 nm for r-HGO-4-29, r-HGO-4-38, and r-HGO-4-46, respectively, suggesting that the reduction decreases the average size of the sp^2 domains and the new sp^2 domains created by the reduction are smaller than the original ones. A similar trend was also observed for the r-HGO-1.25 samples (cf. Figure S1 in the Supporting Information).

The morphology of GO and HGO nanosheets is characterized using AFM. Figure 1d reveals that the GO nanosheets are single-layered with an apparent thickness of ≈ 1 nm and do not have any holes. These nanosheets also have the size larger than 1 micron, which is much greater than the graphitic crystal size. By contrast, the HGO-1 shows holes with an average size of 18 ± 3 nm, and the average hole size increases to 34 ± 7 nm for HGO-2 and 62 ± 19 nm for HGO-3. Exampled holes and profiles are also illustrated in Figure 1d. After 4 h etching, the GO nanosheets were broken into small pieces.

Figure 2 shows the structure and properties of the r-HGO membranes comprising the r-HGO selective layer on polyacrylonitrile (PAN350) UF membranes with a molecular weight cut-off of 150 kDa and pore size of ≈ 30 nm. The–CN groups of PAN can form hydrogen bonds with the carboxyl and hydroxcl groups of HGO, yielding adhesion between between PAN and HGO. As shown in Figure 2a, the PAN350 membrane has a rough surface and a high density of pores. After the HGO deposition and reduction, the surface does not have any pores but shows some wrinkles (cf. Figure 2b), confirming the deposition of the HGO layers. As shown in Figure 2c, the r-HGO membranes exhibit water contact angles between 57° and 68°, higher than PAN (46° ± 2°), further validating the deposition of the r-HG layer. Increasing the HI concentration (or the degree of reduction) generally increases the contact angle because of the

enhanced hydrophobicity of the reduced GO.[35] Interestingly, r-HGO-4-46 exhibits lower water contact angle than r-HGO-4-38, presumably because the reduction by the 46% HI solution might change the surface roughness. However, it is beyond the scope of this study to elucidate such changes.

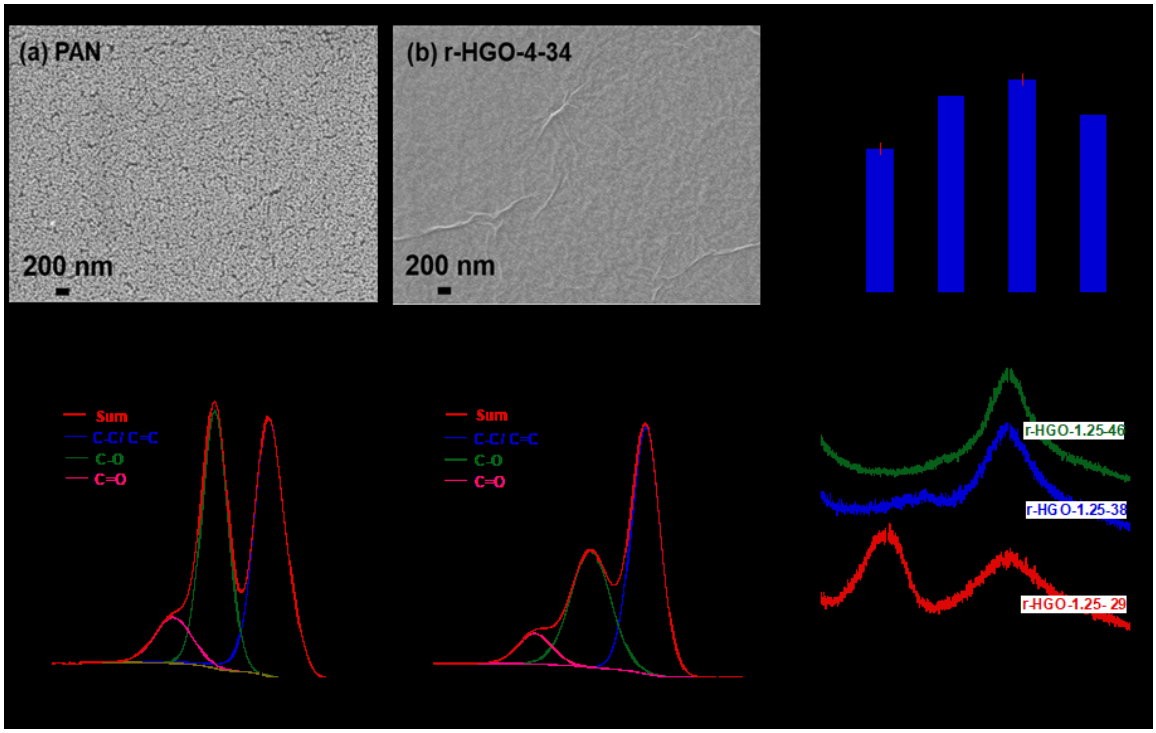

Figure 2. Characterization of r-HGO membranes. Scanning electron microscope (SEM) images of the surface of (a) PAN350 and (b) r-HGO-4-34 (30-nm thick) membrane. (c) Water contact angle on PAN350 and r-HGO-4 membranes. High-resolution C 1s XPS spectra of (d) HGO-1.25 and (e) r-HGO-1.25-29. (f) XRD patterns of HGO-1.25 membranes with different degrees of reduction.

We performed an elemental analysis of the GO, HGO, and r-HGO using x-ray photoelectron spectroscopy (XPS). The C/O atom ratio is 2.3 in GO and increases to 2.8 in HGO-1.25 (cf. Table S1), which first appears to be counterintuitive given that the H_2O_2 etching is an oxidation process. However, the defect regions of the GO often contain significant

amounts of oxygen-containing groups, which can be easily removed during the H_2O_2 etching process, resulting in an increase in the C/O ratio.[22] The reduction further increases the C/O ratio. For example, r-HGO-1.25-29, r-HGO-1.25-34, and r-HGO-1.25-46 exhibit the C/O ratio of 3.6, 4.3, and 6.1, respectively. Figures 2d and 2e compare the C 1S spectra in HGO-1.25 and r-HGO-1.25-29 to elucidate the effect of the reduction on the removal of the O-containing groups. The reduction decreases the C-O content from 40 % to 35 %, increases the C-C/C=C content from 50 % to 55 %, and has no impact on the C=O content, suggesting that the epoxide and hydroxyl groups are easier to be removed than C=O groups during the HI reduction processes.

Figure 2f presents the effect of the reduction on the structure of HGO using x-ray diffraction (XRD) analysis. HGO-1.25 membrane shows a diffraction peak at $2\theta = 11.4°$, corresponding with an interlayer distance of 7.8 Å, consistent with the literature (7.6 Å).[30] The reduction leads to a new peak at $2\theta = 23.1°$ (corresponding with an interlayer space of 3.9 Å), confirming that the reduction decreases the interlayer distance. With increasing degree of reduction, the peak at 11.4° gradually disappears, and the peak at 23.1° becomes more dominant. These results also indicate that the reduction decreases the layer thickness. Assuming all the interlayer space decreases from 7.8 Å to 3.9 Å and a single GO layer remains to be ≈ 1 nm, the reduction can decrease the HGO layer thickness by 22 %.

2.2. Desalination performance of the r-HGO membranes

Figure 3 presents the effect of membrane fabrication and testing conditions on the desalination performance, including the degree of etching and reduction, the thickness of the

HGO layer, and the salt concentration in the feed. As shown in Figure 3a, increasing the etching time increases the water permeance in the membranes of r-HGO-*x*-34 with a thickness of ≈ 16 nm because of the decreased tortuosity (τ) for water transport. The tortuosity in the r-HGO selective layer is estimated as $\tau = \frac{L}{d(1+\sqrt{L^2\rho})}$, where L is the lateral size of r-GO (μm), d is the interlayer distance (μm) between r-GO sheets, and ρ is pore density (μm^{-2}) in r-HGO sheets.[23] For the rGO nanosheets without holes, ρ can be assumed to be 0, and $\tau_0 = L/d$. For the r-HGO samples, $\sqrt{L^2\rho}$ can be assumed to be much greater than 1, and thus, $\tau_H = \frac{1}{d\sqrt{\rho}}$. Threfore, the tortuosity decrease by etching can be expressed as $\tau_0/\tau_H = L\sqrt{\rho}$. With the dimension of ≈1 μm (L) and an assumed ρ value of 1000 μm^{-2}, τ_0/τ_H has a value of 32, consistent with the water permeance increase from 0.4 LMH/bar in rGO to 14 LMH/bar in r-HGO-4-34 by 35 times.[36] Additionally, the $\sqrt{L^2 \times \rho}$ has a value of 32 in this example, validating the assumption of $\sqrt{L^2\rho}$ much greater than 1.

Figure 3a also shows that increasing the etching time decreases the salt rejection. For example, as the etching time increases from 1 h to 4 h, the Na_2SO_4 rejection decreases from 98.5 % to 91.4 %, and the NaCl rejection decreases from 51.8 % to 34.3 % because of the larger pores and smaller sizes of the HGO sheets with increasing degree of etching and more defects generated during the deposition.

Figure 3b presents the water permeance as a function of the r-HGO-4-34 thickness, which is estimated to be 78% of that of the HGO, as shown in Figure 2f. As the thickness of the r-HGO increases from 7.8 nm to 23 nm, the tortuosity of the channels in the r-HGO increase, decreasing water permeance. The permeance of water decreases from 26 to 9.2 LMH/bar, while

the Na_2SO_4 rejection increases from 67.5 % to 96.7 %, and the NaCl rejection increases from 29.9 % to 41.0 %. As expected, the stacking of multiple layers decreases large defects in the selective layers, increasing the salt rejection.

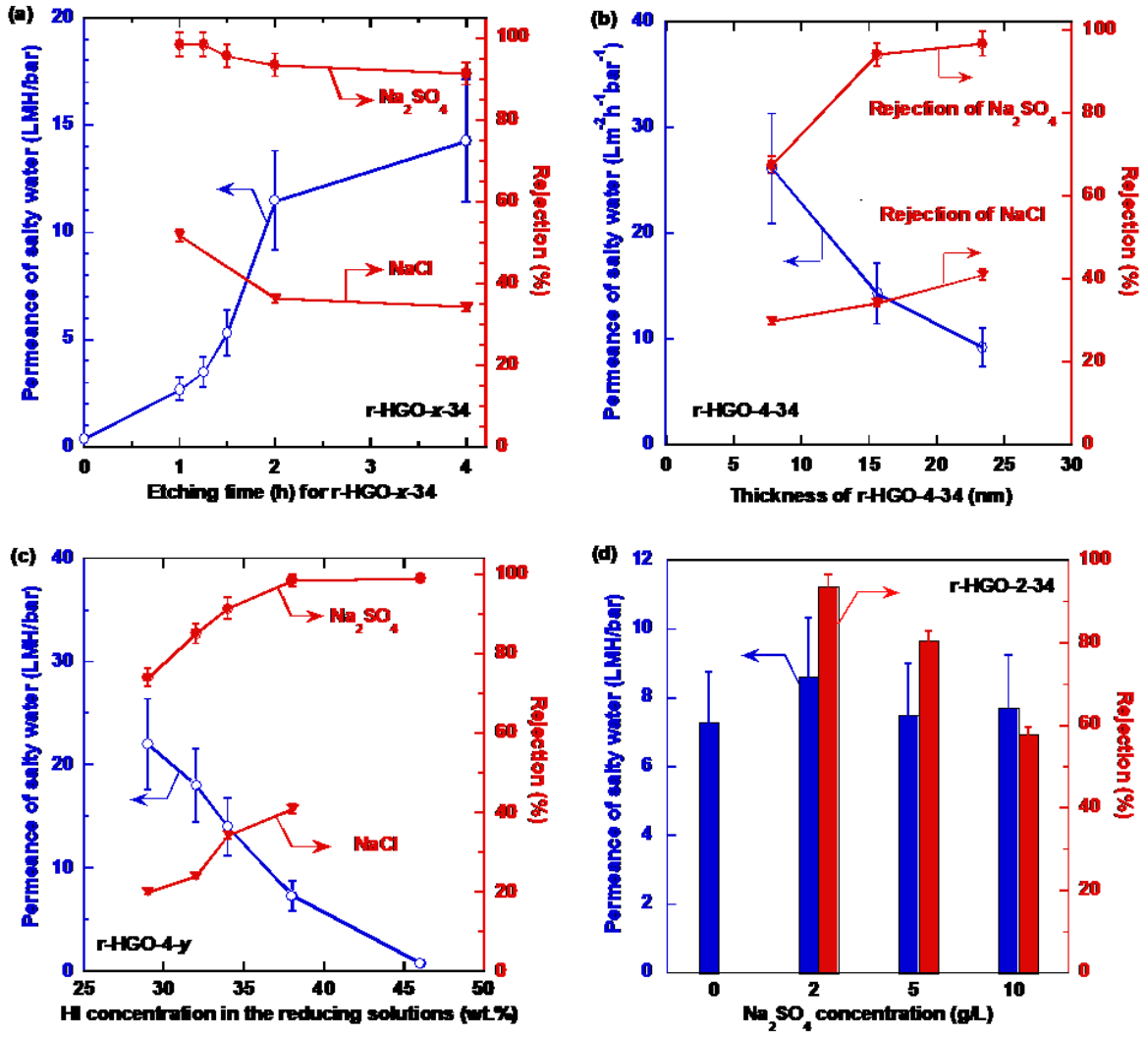

Figure 3. Desalination performance of the r-HGO membranes. Water permeance and salt rejection as a function of (a) the etching time in r-HGO-*x*-34, (b) the film thickness of r-HGO-4-34, (c) the HI concentration in the reducing solutions for the r-HGO-4-*y*, and (d) Na_2SO_4 concentration for r-HGO-2-34. The concentration of the NaCl and Na_2SO_4 solution used in the desalination is 2 g/L in Figure 3a-c. The error bars represent one standard deviation of the data and are taken as the uncertainty of the measurement.

Figure 3c reveals that increasing the degree of reduction decreases the water permeance and increases the salt rejection in the r-HGO-4-*y* membranes. For example, water permeance decreases from 22 LMH/bar in r-HGO-4-29 to 0.77 LMH/bar in r-HGO-4-46 because of the decreased interlay spacing (cf. Figure 2f) and increased hydrophobicity (cf. Figure 2b). Consistently, the Na_2SO_4 rejection increases from 74.0 % in r-HGO-4-29 to 99.1 % in r-HGO-4-46, and the NaCl rejection increases from 20.0 % in r-HGO-4-29 to 34.3 % in r-HGO-4-34. These changes are consistent with the decreased channel size with increasing the reduction degree. For example, the reduction of HGO-1.25 with 46% HI decreases the channel size from 7.8 Å to 3.9 Å, and the trend is expected to be similar for HGO-4 because the degree of etching has minimal effect on the reduction process.

Figure 3d displays that increasing the Na_2SO_4 concentration in the feed decreases its rejection in r-HGO-2-34 but has a negligible effect on the water permeance. When the Na_2SO_4 concentration increases from 2.0 g/L to 10 g/L, the Donnan potential of the negatively charged r-HGO surface decreases, increasing the sorption of co-ions (e.g., SO_4^{2-}) and thus Na_2SO_4 permeability.[19] Consequently, Na_2SO_4 rejection decreases from 93.7 % to 57.9 %. The r-GO-2-34 sample exhibits a water permeance of 8.6±1.7 LMH/bar, lower than that shown in Figure 3a (11.5±2.3 LMH/bar) due to the variance of the samples. On the other hand, the difference is within the uncertainty.

To improve the water permeance, dual-layer of r-HGO membranes were fabricated mimicking the configuration of conventional multi-layer composite membranes to improve permeance. As shown in Figure 4a, a layer of HGO with a higher etching degree (such as

HGO-4) was deposited first, and after drying, the second layer of HGO with a lower etching degree (such as HGO-1) was deposited and then reduced using a 34 % HI solution. The first layer with higher water permeance and moderate selectivity can also serve as a gutter layer to provide a smooth surface for the deposition of the thin second layer with higher salt rejection. The dual-layer membranes are denoted as *m*-*n*, where *m* and *n* are the thickness (nm) of the first layer (HGO-4) and the top layer (HGO-1), respectively.

Figure 4b presents the water permeance and Na_2SO_4 rejection of the representative dual-layer membranes. The membrane 10-2 shows higher water permeance than the 10-3 and comparable Na_2SO_4 rejection, suggesting that the first layer (r-HGO-4-34) has negligible resistance, and r-HGO-1-34 dominates the separation performance. When compared with the 20-0 (r-HGO-4-34 derived from the HGO layer with 20 nm thickness), the 10-2 shows similar Na_2SO_4 rejection and improved water permeance. To further improve the salt rejection, a membrane of 15-5 was prepared, and it shows Na_2SO_4 rejection higher than 10-2 or 10-3 and similar to the 0-20 (r-HGO-1-34), but water permeance much higher than 0-20. Thicker layers are expected to mitigate defects generated during the membrane fabrication. Apparent water permeability was calculated and sown in Figure S3. These results validate the success of the dual-layer approach to achieve superior desalination performance.

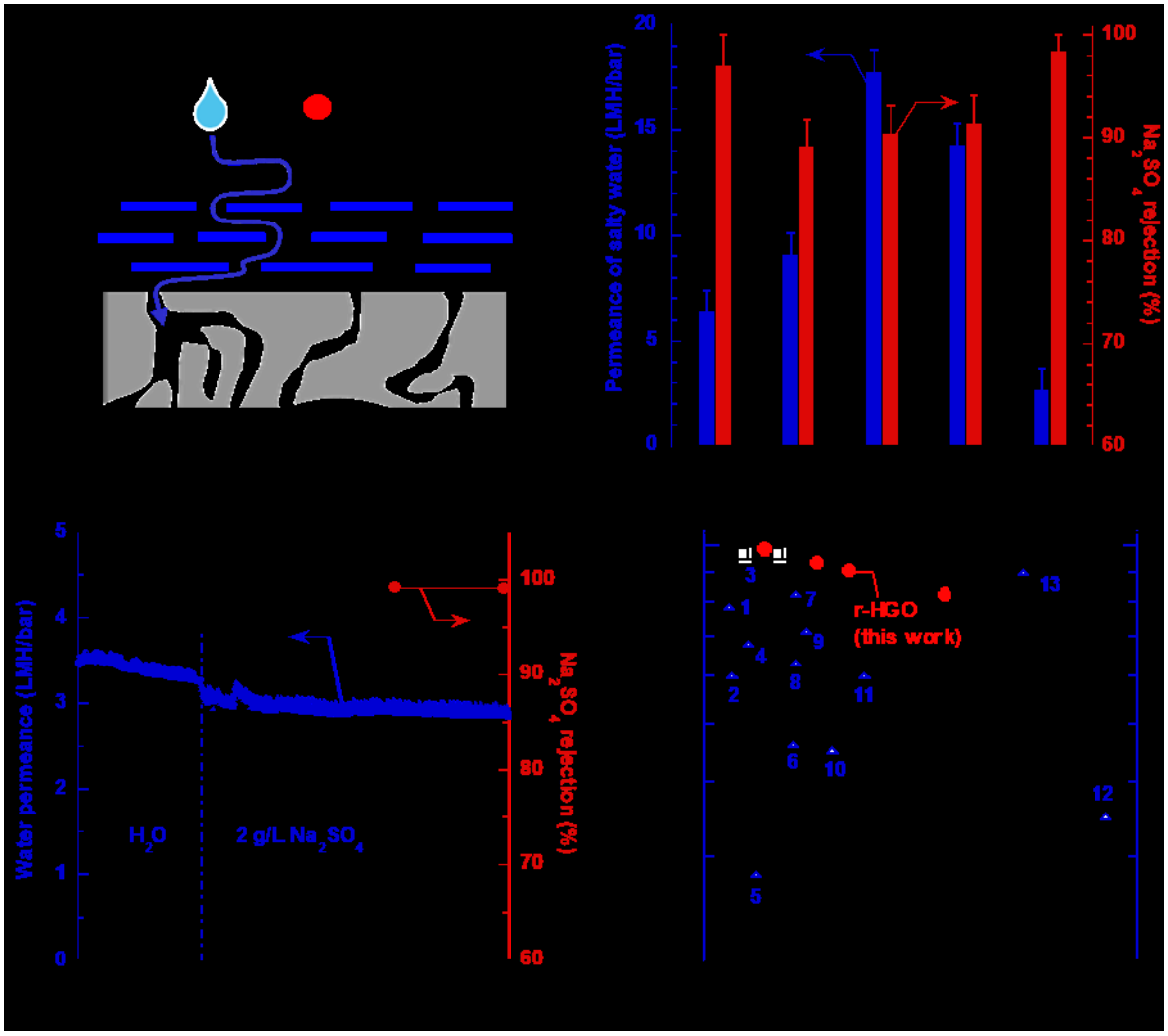

Figure 4. Superior desalination performance of r-HGO membranes. (a) Schematic of dual-layer r-HGO membranes. (b) Water permeance and Na_2SO_4 rejection in representative dual-layer r-HGO membranes of *m-n* (c) Long term stability test of r-HGO-1.25-34 with 2 g/L Na_2SO_4 feed solution at ≈21 ºC. (d) Comparison of the desalination performance of our r-HGO membranes (●) with commercial NF90 and DK4040C1024 membranes[37] (□ for $MgSO_4$) and state-of-the-art GO-based membranes in the literature (Δ).[9, 11, 16, 23, 38-46] The data are also recorded in Table S4.

For the GO-based membranes prepared by vacuum-filtration, there are often concerns that the GO nanosheets may be delaminated by shear force in the crossflow system. To study the stability of r-HGO membranes, we conducted a long term test of r-HGO-1.25-34 in a crossflow system, including a 10 h pure water test at 2.7 bar and 26 h desalination test with 2 g/L Na_2SO_4 at 3.8 bar. The feed flow rate was set to 2 L/min, which corresponds with a Reynolds number

of ≈1800. As shown in Figure 4c, pure-water permeance slightly decreases with time presumably because of the compaction. On the other hand, after 25 h of operation with the saline feed, the membrane exhibits stable water permeance and Na_2SO_4 rejection (≈ 99.2 %), demonstrating the stability of the r-HGO membranes. Although there is no chemical bonding between r-HGO sheets, the π-π bonds between the r-HGO sheets may contributes to the stability of the r-HGO membranes. Especially when the HGO was reduced to r-HGO, the interlayer space of r-HGO was narrowed down to 3.9 Å (as shown in Figure 2f), the π-π interaction turned stronger as a result of the decreasing interlayer space. The stability of the reduced GO has also been reported in the literature.[2, 11, 19, 23]

Figure 4d benchmarks the performance of our r-HGO membranes with the state-of-the-art GO-based membranes reported in the literature. Our r-HGO membranes show higher water permeance than those reported at comparable Na_2SO_4 rejection, demonstrating the promise of our approach in preparing NF membranes. The r-HGO may even be competitive with commercial NF membranes such as NF90.[37] Graphene-based NF membranes have only been studied for a decade, and now their salt rejection and water permeance have simultaneously reached the level of the commercial polyamide-based NF membranes (which have been developed for almost 50 years). Moreover, they were reported to be antibacterial[2, 47, 48] and resistant to aggressive chemical washing.[49-51] Therefore, these r-HGO-based membranes are promising for the next-generation NF membranes.

3. CONCLUSIONS

We demonstrate that the r-HGO can be deposited onto porous supports as thin as several nanometers, and the generation of in-plane nanopores on r-GO sheets using H_2O_2 significantly improve water permeance while retaining high salt rejection. The fabrication conditions (such as etching time, layer thickness, and reduction degree) can be flexibly tuned to achieve a balance of water permeance and salt rejection. For example, an r-HGO-4-34 shows water permeance of 14 LMH/bar and Na_2SO_4 rejection of 91.4 %, while an r-HGO-4-38 shows water permeance of 6.6 LMH/bar and Na_2SO_4 rejection of 98.5 %. The performance is among the best reported for graphene- or GO-based membranes, and it can be further improved by designing multi-layer composite membranes. Moreover, the fabrication of the r-HGO with <10 nm thickness is facile and scalable, making them attractive for practical water purification.

4. EXPERIMENTAL SECTION

Equipment and instruments or materials are identified herein to adequately specify the experimental details. Such identification does not imply recommendation by the National Institute of Standards and Technology, nor does it imply the materials are necessarily the best available for the purpose.

Material. Natural graphite powder (325 mesh) was procured from Qingdao Huatai Graphite Co. (Qingdao, China). H_2SO_4 (99 %), H_2O_2 (30 mass% in H_2O), HI (57 mass% in H_2O), Na_2SO_4 (≥99.0 %), $KMnO_4$ (≥99.0 %), and N, N-dimethylformamide (DMF, 99.8 %) were purchased from Sigma-Aldrich Corporation (St. Louis, MO). HCl (2.0 N) and ethanol (95 %) were supplied by VWR International (Radnor, PA). PAN350 UF membrane was provided by

Sepro Membranes, Inc. (Oceanside, CA). NaCl was obtained from Fisher Scientific International (Hampton, NH).

Fabrication of r-HGO membranes. First, GO was prepared from graphite using a modified Hummers' method.[19] Briefly, 3.0 g graphite was mixed with concentrated H_2SO_4 (70 mL) under agitation at ≈ 22 ºC. 9.0 g $KMnO_4$ was gradually added while the solution was maintained at < 10 ºC using an ice bath. The flask was then transferred to a water bath at 40 ºC, and the solution was stirred for 30 min before adding 150 mL water. The solution was then heated to 90 ºC for 15 min before adding 500 mL water. After that, H_2O_2 solution (30 mass%, 15 mL) was gradually added to remove excessive $KMnO_4$ or manganese dioxide. The solution was filtered, and the precipitated GO was washed with an HCl aqueous solution. The obtained GO was dispersed in distilled water by ultrasonication.

Second, the HGO was prepared by adding 10 mL H_2O_2 in 100 mL 2 g/L GO aqueous solution. The mixture was continuously stirred at 100 °C for various lengths of time (1 h, 2 h, 4 h, or 4.5 h) to obtain different pore sizes and densities. After the reaction, the HGO suspension was purified by centrifugation and vacuum filtration to remove the remaining H_2O_2 and small HGO debris.

Third, the HGO membranes were prepared by vacuum filtration of the HGO aqueous solution on the PAN350 UF membrane. Before the deposition, the PAN350 was pretreated by ethanol for 1 h and then kept in the DI water. The thickness of the HGO layer can be calculated from the mass of HGO in the solution, the density of GO, and the coating area.

Finally, the HGO membranes were dried in air and then reduced by HI solutions [(29 to 46) mass% in water) for 3 h. The obtained r-HGO membrane was washed using running DI water for several hours to remove the residue iodine and then air-dried for 24 h.

Characterization. The prepared GO and HGO were characterized using AFM (Bruker Dimension Icon with ScanAsyst, Bruker, Germany) under tapping mode. The diluted GO or HGO dispersion was dropped on a mica substrate (Ted Pella, Inc., Redding, CA) followed by air drying. XRD was performed using a Rigaku Ultima IV diffractometer (Rigaku, Japan) with Cu Kα radiation (λ= 0.154 nm). FTIR spectrometer (Bruker, Vertex 70 Billerica, MA) was used to characterize the freestanding films of GO and r-HGO. The freestanding films were prepared by immersing the GO or r-HGO membranes in DMF and then transferred to a glass slide. Raman spectra were collected using Raman spectroscopy (Renishaw InVia, UK) with 514 nm laser source. SEM images were obtained using a focused ion beam SEM (FIB-SEM, Carl Zeiss Auriga CrossBeam, Carl Zeiss Germany). XPS was used for elemental analysis of the GOs with a Kratos AXIS Ultra DLD Spectrometer (Kratos Analytical, Manchester, UK) and a monochromatic Al Kα source (1486.6 eV) operating at 140 W. The spectra were collected from a nominal spot size of 300 μm × 700 μm and analyzed using the CasaXPS software package. The water contact angle of the membranes was measured using a Ramé Hart contact angle goniometer (Model 190, Succasunna, NJ).

Water permeance through membranes was determined via dead-end filtration using 2 g/L NaCl or Na_2SO_4 solutions at a feed pressure of 4.0 bar. Water permeance (A_w) was calculated using equation 1:

$$A_w = \frac{V}{A_m \cdot t \cdot (\Delta p - \Delta \pi)} \quad (1)$$

where V (L) is the volume of water permeated through the membrane with an active area of A_m (11.3 cm^2) during a time of t (h), Δp (bar) is the trans-membrane pressure, and $\Delta \pi$ (bar) is the osmotic pressure difference. For salty water, π can be estimated using equation 2:

$$\pi = ncRT \quad (2)$$

where n is the number of ions for each salt molecule, c is the salt concentration in the solution (mol/L), R is the gas constant, and T (K) is the temperature. The salt rejection (R_S, %) can be calculated using equation 3:

$$R_S = \left(1 - \frac{c_p}{c_f}\right) \times 100 \quad (3)$$

where c_p and c_f are the salt concentration in the permeate and feed, respectively. The salt concentration was determined using a conductivity probe (Vernier, OR, US).

The membranes were also tested using a constant-flux crossflow system to demonstrate the long-term stability of r-HGO membrane in the presence of shear force. The feed pressure was kept constant, while the permeate pressure was varied to maintain the targeted permeate flux (controlled by a mass flow controller).

■ ASSOCIATED CONTENT

Supporting Information

The Supporting Information is available free of charge on the ACS Publications website. Experimental details, additional characterization data, and comparison with the state-of-the-art membranes for desalination.

■ AUTHOR INFORMATION

Corresponding Author

*E-mail: haiqingl@buffalo.edu (H. Lin) and lhuang28@buffalo.edu (L. Huang)

ORCID

Haiqing Lin: 0000-0001-8042-154X

Author Contributions

The manuscript was prepared through the contributions of all authors. All authors have approved the final version of the manuscript.

Notes

The authors declare no competing financial interest.

■ ACKNOWLEDGMENTS

We acknowledge the financial support from the U.S. National Science Foundation (NSF) with Award No. 1635026 and the U.S. Department of Interior with Award No. R17AC00147. This work is an official contribution of the National Institute of Standards and Technology and not subject to copyright in the United States.

■ REFERENCES

1. Anand, A.; Unnikrishnan, B.; Mao, J.; Lin, H.; Huang, C., Graphene-based Nanofiltration Membranes for Improving Salt Rejection, Water Flux and Antifouling-A Review. *Desalination* **2018,** *429*, 119-133.

2. Yousefi, N.; Lu, X.; Elimelech, M.; Tufenkji, N., Environmental Performance of Graphene-based 3D Macrostructures. *Nat. Nanotechnol.* **2019,** *14* (2), 107-119.
3. Liu, G.; Jin, W.; Xu, N., Graphene-Based Membranes. *Chem. Soc. Rev.* **2015,** *44*, 5016-5030.
4. Surwade, S. P.; Smirnov, S. N.; Vlassiouk, I. V.; Unocic, R. R.; Veith, G. M.; Dai, S.; Mahurin, S. M., Water Desalination Using Nanoporous Single-Layer Graphene. *Nat. Nanotechnol.* **2015,** *10* (5), 459-464.
5. Cohen-Tanugi, D.; Lin, L.; Grossman, J. C., Multilayer Nanoporous Graphene Membranes for Water Desalination. *Nano Lett.* **2016,** *16* (2), 1027-1033.
6. Yang, Y.; Yang, X.; Liang, L.; Gao, Y.; Cheng, H.; Li, X.; Zou, M.; Ma, R.; Yuan, Q.; Duan, X., Large-Area Graphene-Nanomesh/Carbon-Nanotube Hybrid Membranes for Ionic and Molecular Nanofiltration. *Science* **2019,** *364* (6445), 1057-1062.
7. O'Hern, S. C.; Boutilier, M. S. H.; Idrobo, J. C.; Song, Y.; Kong, J.; Laoui, T.; Atieh, M.; Karnik, R., Selective Ionic Transport through Tunable Subnanometer Pores in Single-Layer Graphene Membranes. *Nano Lett.* **2014,** *14* (3), 1234-1241.
8. Mi, B., Scaling up Nanoporous Graphene Membranes. *Science* **2019,** *364* (6445), 1033-1034.
9. Hu, M.; Mi, B., Enabling Graphene Oxide Nanosheets as Water Separation Membranes. *Environ. Sci. Technol.* **2013,** *47* (8), 3715-3723.
10. Mi, B.; Zheng, S.; Tu, Q., 2D Graphene Oxide Channel for Water Transport. *Faraday Discuss.* **2018,** *209*, 329-340.
11. Chang, Y.; Shen, Y.; Kong, D.; Ning, J.; Xiao, Z.; Liang, J.; Zhi, L., Fabrication of the Reduced Preoxidized Graphene-Based Nanofiltration Membranes with Tunable Porosity and Good Performance. *RSC Adv.* **2017,** *7* (5), 2544-2549.
12. Buelke, C.; Alshami, A.; Casler, J.; Lin, Y.; Hickner, M.; Aljundi, I. H., Evaluating Graphene Oxide and Holey Graphene Oxide Membrane Performance for Water Purification. *J. Membr. Sci.* **2019,** *588*, 117195.
13. Ying, Y.; Sun, L.; Wang, Q.; Fan, Z.; Peng, X., In-Plane Mesoporous Graphene Oxide Nanosheet Assembled Membranes for Molecular Separation. *RSC Adv.* **2014,** *4* (41), 21425-21428.
14. Kim, D.; Choi, J.; Kim, D.; Jung, H.-T., Enhanced Water Permeation Based on Nanoporous Multilayer Graphene Membranes: the Role of Pore Size and Density. *J. Mater. Chem. A* **2016,** *4* (45), 17773-17781.
15. Joshi, R. K.; Carbone, P.; Wang, F.; Kravets, V. G.; Su, Y.; Grigorieva, I. V.; Wu, H.; Geim, A. K.; Nair, R. R., Precise and Ultrafast Molecular Sieving through Graphene Oxide Membranes. *Science* **2014,** *343* (6172), 752-754.
16. Xu, W.; Fang, C.; Zhou, F.; Song, Z.; Liu, Q.; Qiao, R.; Yu, M., Self-Assembly: A Facile Way of Forming Ultrathin, High-Performance Graphene Oxide Membranes for Water Purification. *Nano Lett.* **2017,** *17* (5), 2928-2933.
17. Chen, L.; Shi, G.; Shen, J.; Peng, B.; Zhang, B.; Wang, Y.; Bian, F.; Wang, J.; Li, D.; Qian, Z.; Xu, G.; Liu, G.; Zeng, J.; Zhang, L.; Yang, Y.; Zhou, G.; Wu, M.; Jin, W.; Li, J.;

Fang, H., Ion Sieving in Graphene Oxide Membranes via Cationic Control of Interlayer Spacing. *Nature* **2017,** *550* (7676), 415-418.
18. Huang, K.; Liu, G.; Lou, Y.; Dong, Z.; Shen, J.; Jin, W., A Graphene Oxide Membrane with Highly Selective Molecular Separation of Aqueous Organic Solution. *Angew. Chem. Int. Ed.* **2014,** *53* (27), 6929-6932.
19. Huang, L.; Huang, S.; Venna, S. R.; Lin, H., Rightsizing Nanochannels in Reduced Graphene Oxide Membranes by Solvating for Dye Desalination. *Environ. Sci. Technol.* **2018,** *52* (21), 12649-12655.
20. Yang, E.; Ham, M.; Park, H.; Kim, C.; Song, J.; Kim, I., Tunable Semi-Permeability of Graphene-Based Membranes by Adjusting Reduction Degree of Laminar Graphene Oxide Layer. *J. Membr. Sci.* **2018,** *547*, 73-79.
21. Thebo, K. H.; Qian, X.; Zhang, Q.; Chen, L.; Cheng, H.-M.; Ren, W., Highly Stable Graphene-Oxide-Based Membranes with Superior Permeability. *Nat. Commun.* **2018,** *9* (1), 1486.
22. Xu, Y.; Chen, C.-Y.; Zhao, Z.; Lin, Z.; Lee, C.; Xu, X.; Wang, C.; Huang, Y.; Shakir, M. I.; Duan, X., Solution Processable Holey Graphene Oxide and Its Derived Macrostructures for High-Performance Supercapacitors. *Nano Lett.* **2015,** *15* (7), 4605-4610.
23. Li, Y.; Zhao, W.; Weyland, M.; Yuan, S.; Xia, Y.; Liu, H.; Jian, M.; Yang, J.; Easton, C. D.; Selomulya, C.; Zhang, X., Thermally Reduced Nanoporous Graphene Oxide Membrane for Desalination. *Environ. Sci. Technol.* **2019,** *53* (14), 8314-8323.
24. Zan, R.; Ramasse, Q. M.; Bangert, U.; Novoselov, K. S., Graphene Reknits Its Holes. *Nano Lett.* **2012,** *12* (8), 3936-3940.
25. Koenig, S. P.; Wang, L.; Pellegrino, J.; Bunch, J. S., Selective Molecular Sieving through Porous Graphene. *Nat. Nanotechnol.* **2012,** *7* (11), 728-732.
26. Zhou, D.; Cui, Y.; Xiao, P.; Jiang, M.; Han, B., A General and Scalable Synthesis Approach to Porous Graphene. *Nat. Commun.* **2014,** *5*, 4716.
27. Lin, Y.; Watson, K. A.; Kim, J.-W.; Baggett, D. W.; Working, D. C.; Connell, J. W., Bulk Preparation of Holey Graphene via Controlled Catalytic Oxidation. *Nanoscale* **2013,** *5* (17), 7814-7824.
28. Kim, H.; Yoon, H.; Yoon, S.-M.; Yoo, B.; Ahn, B.; Cho, Y.; Shin, H.; Yang, H.; Paik, U.; Kwon, S.; Choi, J.-Y.; Park, H., Selective Gas Transport through Few-Layered Graphene and Graphene Oxide Membranes. *Science* **2013,** *342* (6154), 91-95.
29. Su, C.; Tandiana, R.; Balapanuru, J.; Tang, W.; Pareek, K.; Nai, C.; Hayashi, T.; Loh, K., Tandem Catalysis of Amines Using Porous Graphene Oxide. *J. Am. Chem. Soc.* **2015,** *137* (2), 685-690.
30. Su, C.; Acik, M.; Takai, K.; Lu, J.; Hao, S.-j.; Zheng, Y.; Wu, P.; Bao, Q.; Enoki, T.; Chabal, Y. J.; Loh, K., Probing the Catalytic Activity of Porous Graphene Oxide and the Origin of This Behaviour. *Nat. Commun.* **2012,** *3*, 1298.
31. Chu, K.; Fathizadeh, M.; Yu, M.; Flora, J. R. V.; Jang, A.; Jang, M.; Park, C.; Yoo, S.; Her, N.; Yoon, Y., Evaluation of Removal Mechanisms in a Graphene Oxide-Coated Ceramic Ultrafiltration Membrane for Retention of Natural Organic Matter,

Pharmaceuticals, and Inorganic Salts. *ACS Appl. Mater. Interfaces* **2017,** *9* (46), 40369-40377.
32. Zheng, S.; Tu, Q.; Urban, J. J.; Li, S.; Mi, B., Swelling of Graphene Oxide Membranes in Aqueous Solution: Characterization of Interlayer Spacing and Insight into Water Transport Mechanisms. *ACS Nano* **2017,** *11* (6), 6440-6450.
33. Ferrari, A. C.; Basko, D. M., Raman Spectroscopy as a Versatile Tool for Studying the Properties of Graphene. *Nat. Nanotechnol.* **2013,** *8* (4), 235-246.
34. Abeykoon, N. C.; Garcia, V.; Jayawickramage, R. A.; Perera, W.; Cure, J.; Chabal, Y. J.; Balkus, K. J.; Ferraris, J. P., Novel Binder-Free Electrode Materials for Supercapacitors Utilizing High Surface Area Carbon Nanofibers Derived from Immiscible Polymer Blends of PBI/6FDA-DAM: DABA. *RSC Adv.* **2017,** *7* (34), 20947-20959.
35. Hu, X.; Yu, Y.; Hou, W.; Zhou, J.; Song, L., Effects of Particle Size and pH Value on the Hydrophilicity of Graphene Oxide. *Appl. Surf. Sci.* **2013,** *273*, 118-121.
36. Karan, S.; Samitsu, S.; Peng, X.; Kurashima, K.; Ichinose, I., Ultrafast Viscous Permeation of Organic Solvents through Diamond-Like Carbon Nanosheets. *Science* **2012,** *335* (6067), 444-447.
37. Kamcev, J.; Freeman, B. D., Nanofiltration Membranes. In *Encyclopedia of Polymeric Nanomaterials*, Kobayashi, S.; Müllen, K., Eds. Springer Berlin Heidelberg: Berlin, Heidelberg, 2021; pp 1-9.
38. Baskoro, F.; Wong, C.-B.; Kumar, S. R.; Chang, C.-W.; Chen, C.-H.; Chen, D. W.; Lue, S. J., Graphene Oxide-Cation Interaction: Inter-layer Spacing and Zeta Potential Changes in Response to Various Salt Solutions. *J. Membr. Sci.* **2018,** *554*, 253-263.
39. Han, Y.; Jiang, Y.; Gao, C., High-Flux Graphene Oxide Nanofiltration Membrane Intercalated by Carbon Nanotubes. *ACS Appl. Mater. Interfaces* **2015,** *7* (15), 8147-8155.
40. Oh, Y.; Armstrong, D. L.; Finnerty, C.; Zheng, S.; Hu, M.; Torrents, A.; Mi, B., Understanding the pH-Responsive Behavior of Graphene Oxide Membrane in Removing Ions and Organic Micropollulants. *J. Membr. Sci.* **2017,** *541*, 235-243.
41. Zhu, L.; Wang, H.; Bai, J.; Liu, J.; Zhang, Y., A Porous Graphene Composite Membrane Intercalated by Halloysite Nanotubes for Efficient Dye Desalination. *Desalination* **2017,** *420*, 145-157.
42. Zhang, H.; Quan, X.; Chen, S.; Fan, X.; Wei, G.; Yu, H., Combined Effects of Surface Charge and Pore Size on Co-enhanced Permeability and Ion Selectivity through RGO-OCNT Nanofiltration Membranes. *Environ. Sci. Technol.* **2018,** *52* (8), 4827-4834.
43. Chen, L.; Moon, J.-H.; Ma, X.; Zhang, L.; Chen, Q.; Chen, L.; Peng, R.; Si, P.; Feng, J.; Li, Y.; Lou, J.; Ci, L., High Performance Graphene Oxide Nanofiltration Membrane Prepared by Electrospraying for Wastewater Purification. *Carbon* **2018,** *130*, 487-494.
44. Ganesh, B. M.; Isloor, A. M.; Ismail, A. F., Enhanced Hydrophilicity and Salt Rejection Study of Graphene Oxide-Polysulfone Mixed Matrix Membrane. *Desalination* **2013,** *313*, 199-207.
45. Han, Y.; Xu, Z.; Gao, C., Ultrathin Graphene Nanofiltration Membrane for Water Purification. *Adv. Funct. Mater.* **2013,** *23* (29), 3693-3700.

46. Akbari, A.; Sheath, P.; Martin, S. T.; Shinde, D. B.; Shaibani, M.; Banerjee, P. C.; Tkacz, R.; Bhattacharyya, D.; Majumder, M., Large-Area Graphene-Based Nanofiltration Membranes by Shear Alignment of Discotic Nematic Liquid Crystals of Graphene Oxide. *Nat. Commun.* **2016,** *7*, 10891.
47. Lu, X.; Feng, X.; Werber, J. R.; Chu, C.; Zucker, I.; Kim, J.-H.; Osuji, C. O.; Elimelech, M., Enhanced Antibacterial Activity through the Controlled Alignment of Graphene Oxide Nanosheets. *Proc. Natl. Acad. Sci. U.S.A.* **2017,** *114* (46), E9793-E9801.
48. Zhang, W.; Yang, Y.; Ziemann, E.; Be'er, A.; Bashouti, M. Y.; Elimelech, M.; Bernstein, R., One-Step Sonochemical Synthesis of a Reduced Graphene Oxide–ZnO Nanocomposite with Antibacterial and Antibiofouling Properties. *Environ. Sci. Nano* **2019,** *6*, 3080-3090.
49. Miao, W.; Li, Z.-K.; Yan, X.; Guo, Y.-J.; Lang, W.-Z., Improved Ultrafiltration Performance and Chlorine Resistance of PVDF Hollow Fiber Membranes via Doping with Sulfonated Graphene Oxide. *Chem. Eng. J.* **2017,** *317*, 901-912.
50. Shao, F.; Dong, L.; Dong, H.; Zhang, Q.; Zhao, M.; Yu, L.; Pang, B.; Chen, Y., Graphene Oxide Modified Polyamide Reverse Osmosis Membranes with Enhanced Chlorine Resistance. *J. Membr. Sci.* **2017,** *525*, 9-17.
51. Zhang, C.; Wei, K.; Zhang, W.; Bai, Y.; Sun, Y.; Gu, J., Graphene Oxide Quantum Dots Incorporated into a Thin Film Nanocomposite Membrane with High Flux and Antifouling Properties for Low-Pressure Nanofiltration. *ACS Appl. Mater. Interfaces* **2017,** *9* (12), 11082-11094.

Graphic Abstract